Available online at www.sciencedirect.com
ScienceDirect
Trans. Nonferrous Met. Soc. China 35(2025) 4149−4165
Transactions of Nonferrous Metals Society of China
www.tnmsc.cn

Isotropic evolution features during ultrasonic welding of Cu single crystals

Qiu-chen MA[1,2,3], Jing-yuan MA[2,3], Xiao-xiong ZHENG[2,3], Xu-kai HUANG[1], Hong-jun JI[2,3]

1. School of Advanced Manufacturing, Fuzhou University, Jinjiang 362251, China;
2. State Key Laboratory of Precision Welding & Joining of Materials and Structures, Harbin Institute of Technology at Shenzhen, Shenzhen 518055, China;
3. School of Integrated Circuits, Harbin Institute of Technology at Shenzhen, Shenzhen 518055, China

Received 14 March 2024; accepted 13 November 2024

Abstract: Based on the relationship between deformation microstructures and grain orientations, three characteristic Cu single crystals were used to investigate the opposite effects of ultrasonic superimposed high-strain-rate on the dislocation motion during ultrasonic welding (UW). The results revealed that equiaxed dislocation cells and discontinuous dynamic recrystallization (DRX) grains dominated in the joint microstructures. Three Cu single crystal joints exhibited an isotropic trend in grain orientation, welding quality, and microscopic mechanical properties. The preferred dislocation behaviors and DRX modes were further analyzed by modelling the stored energy difference, indicating that high mobility of intra-granular dislocations and homogeneous dislocation motion induced by the ultrasonic excitation were the intrinsic factors contributing to the formation of isotropic microstructures and welding quality.

Key words: Cu single crystal; ultrasonic welding; dynamic recrystallization; dislocation substructure; high-strain-rate deformation

1 Introduction

Ultrasonic welding (UW) is a rapid solid-state bonding technology widely applied in integrated circuits, power electronics, and lithium-ion battery manufacturing. By employing normal force and interfacial reciprocal sliding, a robust weld is typically formed within 1 s [1]. During UW, the high-frequency relative motion between upper and lower substrate parts leads to a dynamic weld formation process, including micro-weld formation, deformation, breakage, and re-bonding [2−4]. The high-strain-rate deformation in the interfacial regions leads to unique phenomena during UW, such as enhanced elemental diffusion [5], massive vacancy formation [6], amorphization [7], and phase-transformation-induced weld formation [8]. Unlike the rapid accumulation and severe interaction of dislocations caused by high-strain-rate deformation, ultrasonic excitation mitigates dislocation pile-up and facilitates the sub-grain formation [9,10]. However, the mechanisms underlying the interaction of ultrasonic excitation and high-strain-rate deformation on microstructural evolution during UW remain unclear.

Cu, as a metal with medium stacking fault energy, exhibits various dislocation behaviors, such as planar slip, cross-slip or twinning, depending on the plastic deformation conditions [11]. BROWN et al [12] manipulated the Zener–Hollomon parameter (Z parameter) to design diverse deformation modes

Corresponding author: Qiu-chen MA, Tel: +86-13612879156, E-mail: maqc@fzu.edu.cn;
Hong-jun JI, E-mail: jhj7005@hit.edu.cn
https://doi.org/10.1016/S1003-6326(25)66935-4

for microcrystalline Cu, and observed a preference for the formation of deformation twins when the $\ln Z$ value exceeded 31. WINTHER et al [13,14] investigated the effect of matrix orientation on dislocation substructures in terms of active slip systems using quasi-static tension for pure Cu, identifying preferred matrix orientations for forming geometrically necessary boundaries (GNBs) and incidental dislocation boundaries (IDBs). CAI et al [15] and VOISIN et al [16] explored the orientation dependence during high-strain-rate deformation, revealing a correlation between dislocation substructures and grain orientation in the twinning refinement mode induced by dislocation pile-up.

In contrast to severe dislocation entanglements induced by orientation constraints or high-strain-rate deformation, dislocation dynamics simulations conducted by SIU et al [17] and BACHURIN et al [18] revealed that ultrasonic excitation promoted dislocation dipole annihilation by enhancing dislocation drifting. KANG et al [19,20] combined visco-plastic self-consistent model and quasi-static tension test for pure Cu, and illustrated an anisotropic softening phenomenon in the deformed grains with various orientations under the ultrasonic vibration. The interfacial deformation during UW presents a complex loading mode of ultrasonic superimposed on the high-strain-rate. Instead of massive deformation twins under the conventional high-strain-rate deformation, the characterization results of NI et al [21] found that only a few nano-sized twins occurred in local interfacial regions of the Cu−Ni ultrasonically welded joints. Notably, even in ultrasonically welded low-carbon Fe or Ti joints [8,22], where the slip systems were more restricted, deformation twins were rarely found or discussed.

In summary, the deformation condition in the interfacial regions during UW involves a complex loading mode of ultrasonic superimposed high-strain-rate. Different impacts of ultrasonic vibration and high-strain-rate on the microstructure evolution at the ultrasonically welded interfaces require further analysis. In this research, based on the correlation between orientation and deformation microstructures, the evolution of interfacial microstructures and welding quality was traced and analyzed using three characteristic Cu single crystals. Dislocation and dynamic recrystallization (DRX) behaviors of joints with various orientations were simultaneously investigated using transmission Kikuchi diffraction (TKD) and transmission electron microscopy (TEM). X-ray computed tomography (X-CT) and nano-indentation tests were performed to evaluate the orientation dependence of bonding quality. Preferred dislocation behaviors and DRX modes under the ultrasonic superimposed high-strain-rate deformation were further discussed by establishing a numerical model of stored energy difference.

2 Experimental

The Cu single crystal substrates with dimensions of 10 mm × 5 mm × 1 mm were used for UW. The orientations and mechanical properties were analyzed using electron backscatter diffraction (EBSD) and nano-indentation, respectively, as shown in Figs. 1 and 2. The inverse pole figures (IPFs) and pole figures (PFs) indicated that the initial Cu single crystals exhibited highly uniform [001], [101], and [111] orientations. The misorientation profiles (Figs. 2(a−c)) confirmed the absence of high-angle grain boundaries (HAGBs) or low-angle grain boundaries (LAGBs) in the initial Cu single crystals. The microhardness values of the Cu single crystals with [001], [101], and [111] orientations were HV 103.1, HV 103.3, and HV 111.4, respectively, which were consistent with the correlation between grain orientations and mechanical properties ([111] > [101] ≈ [001]) [23].

The welding surfaces were ground, polished, and cleaned in ethanol before UW. The Cu single crystals with the same orientation were stacked and welded using an ultrasonic welder (Branson Ultraweld L20). Both the sonotrode and anvil featured pyramidal tip patterns, with the sonotrode tip truncated to a surface area of 0.09 mm^2 and anvil side to 0.04 mm^2. Based on the EBSD analysis, the rolling direction (RD), transverse direction (TD), and normal direction (ND) shown in Fig. 2(d) corresponded to $[1\bar{1}0]/[110]/[001]$, $[12\bar{1}]/[\bar{1}11]/[101]$, and $[1\bar{2}1]/[10\bar{1}]/[111]$ for [001], [101], and [111]-oriented substrates, respectively.

As shown in Table 1, the primary welding parameters of welding pressure (0.31 MPa), vibration frequency (20 kHz) and oscillation amplitude (55 μm) were kept constant during UW, with welding energies of 200 and 700 J. Before

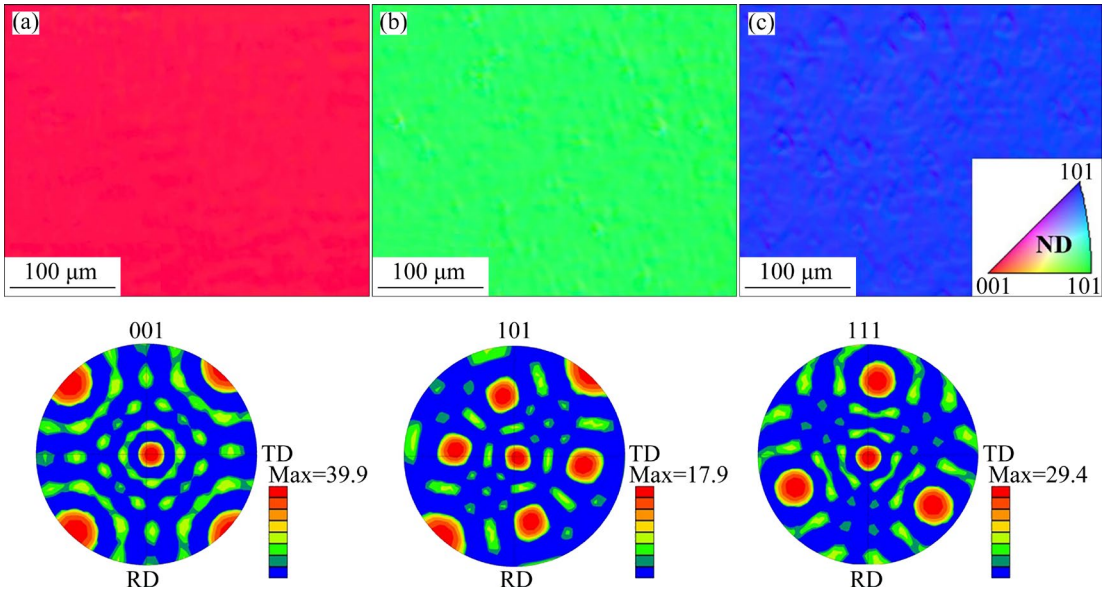

Fig. 1 EBSD results of Cu single crystals with [001] (a), [101] (b), and [111] (c) orientations

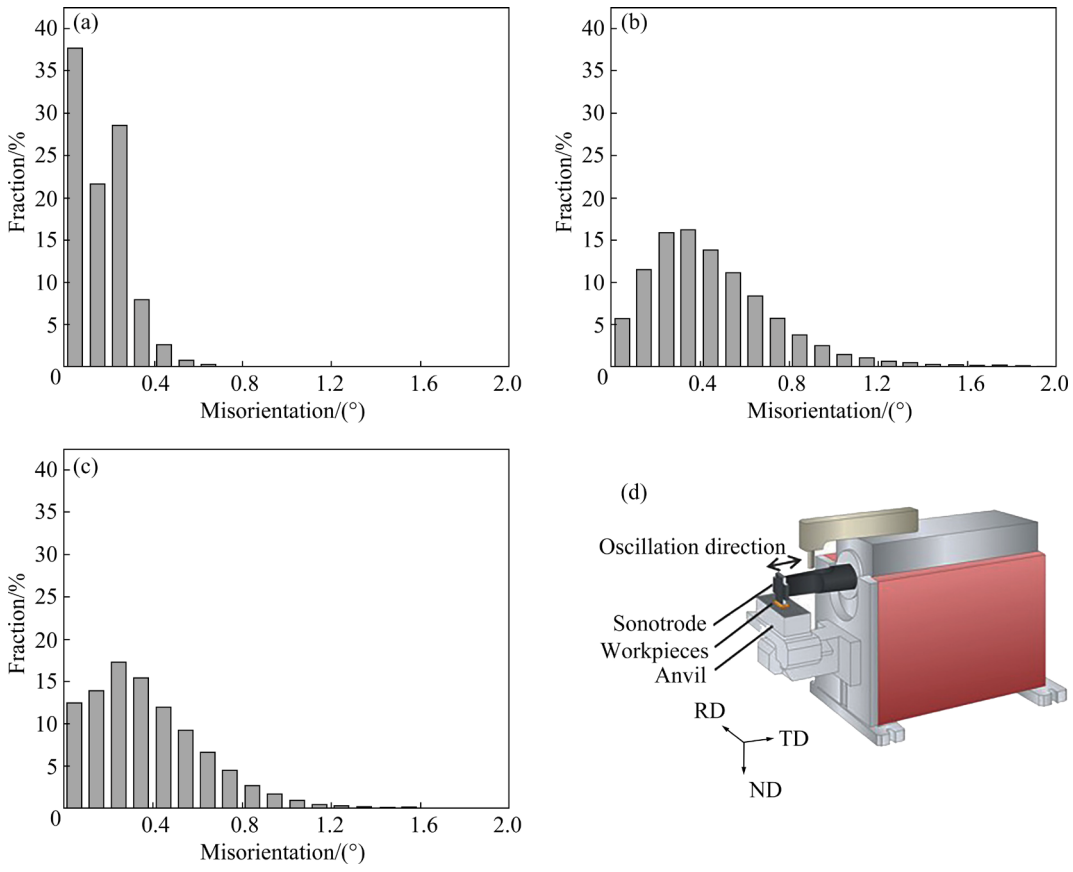

Fig. 2 Misorientation profiles of Cu single crystals with [001] (a), [101] (b), and [111] (c) orientations; (d) Welding configuration of Cu single crystals

microstructural characterization, the ND−TD planes of the joints were prepared through grinding, mechanical polishing, and electrolytic polishing. The orientation evolution of Cu single crystals was characterized using an X-ray diffractometer (XRD, DMAX2500). Low-magnification EBSD characterization, using a step size of 0.8 μm and a voltage of 20 kV, involved scanning the electron beam in the TD−ND plane. High-magnification TKD characterization was performed on samples

Table 1 Specific parameters for UW of Cu single crystals

Orientation	Welding energy/J	Welding pressure/MPa	Welding time/s	Vibration frequency/kHz	Oscillation amplitude/μm	Power/W
[001]	200	0.31	0.26	20	55	1450
[101]	200	0.31	0.31	20	55	1320
[111]	200	0.31	0.29	20	55	1380
[001]	700	0.31	0.61	20	55	1580
[101]	700	0.31	0.60	20	55	1660
[111]	700	0.31	0.59	20	55	1700

prepared with a standard lift-out method using a dual-beam field emission scanning electron microscope (FE-SEM, Helios G4 CX), with analysis conducted in the RD−ND plane at a step size of 30 nm and a voltage of 30 kV. EBSD and TKD data were processed using OIM analysis software. Dislocation substructures and nano-sized DRX grains were observed using TEM and scanning transmission electron microscopy (STEM) on a 200 kV JEOL−2100F instrument. The Vickers microhardness of the ultrasonically welded joints was measured with a KLA G200X nanoindentation system, ensuring thermal drift calibration for precision and setting indentation spacing to ten times the maximum depth. The interfacial welding quality was assessed using X-ray computed tomography (X-CT; Zeiss Xradia 515 Versa) at 140 kV, with an exposure time of 2 s and a pixel size of 6 μm.

3 Results

3.1 Macro-weld evolution at interfaces

Under low welding energy inputs, the interfacial regions directly below the knurl pattern tips of the sonotrode preferentially formed local welds. Correspondingly, the interfacial microstructures characterized by EBSD at low magnification were selected from these regions. Figure 3 represents the low-magnification EBSD characterization results of Cu single crystal joints with [001], [101], and [111] orientations. The locations of interface and DRX grains were marked by the black arrows. At a low welding energy input of 200 J, high-frequency friction drove the initial flat interface to a serrated morphology, which provided potential sites for the nucleation of subsequent recrystallization.

SAKAI et al [24] indicated that DRX was a grain refinement process driven by the coupling of thermal and stress. Because of insufficient accumulation of stored strain energy and frictional heat, only several DRX grains appeared along the mutual contact surfaces. Moreover, based on the orientation dependence proposed by WINTHER et al [13,14], the limited development of slip systems resulted in parallel GNBs in Cu single crystals with [101] and [111] orientations. Surprisingly, there was no obvious discrepancy in the plastic deformation and recrystallization behavior for ultrasonically welded joints of Cu single crystals, which was further analyzed and discussed in the following section.

In Figs. 3(d−f), the color scale in IPF maps indicated that the enhanced frictional deformation caused by a higher energy input of 700 J led to the formation of wavy GNBs, primarily in the adjacent areas of [111] joints. AN et al [25] suggested that GNBs were derived from the accommodation of shear strain gradients during inhomogeneous deformation. Moreover, with the increase in the number of symmetric slip systems, the dislocation substructures transformed gradually from parallel GNBs to wavy GNBs and equiaxed dislocation cells. In contrast to the orientation-constrained dislocation behaviors, the molecular dynamics simulation of ultrasonic-assisted tension for monocrystalline Cu by ZHAO et al [26] proposed that ultrasonic vibration facilitated the motion and annihilation of dislocations by enhancing atomic kinetic energy. For ultrasonic superimposed high-strain-rate deformation in this research, even in the [111] joints, where the slip systems were most restricted, the wavy GNBs were still observed because of enhanced dislocation motion.

In the interfacial regions of single crystal joints welded at 700 J, the expansion of DRX grains toward the unwelded regions and adjacent areas of

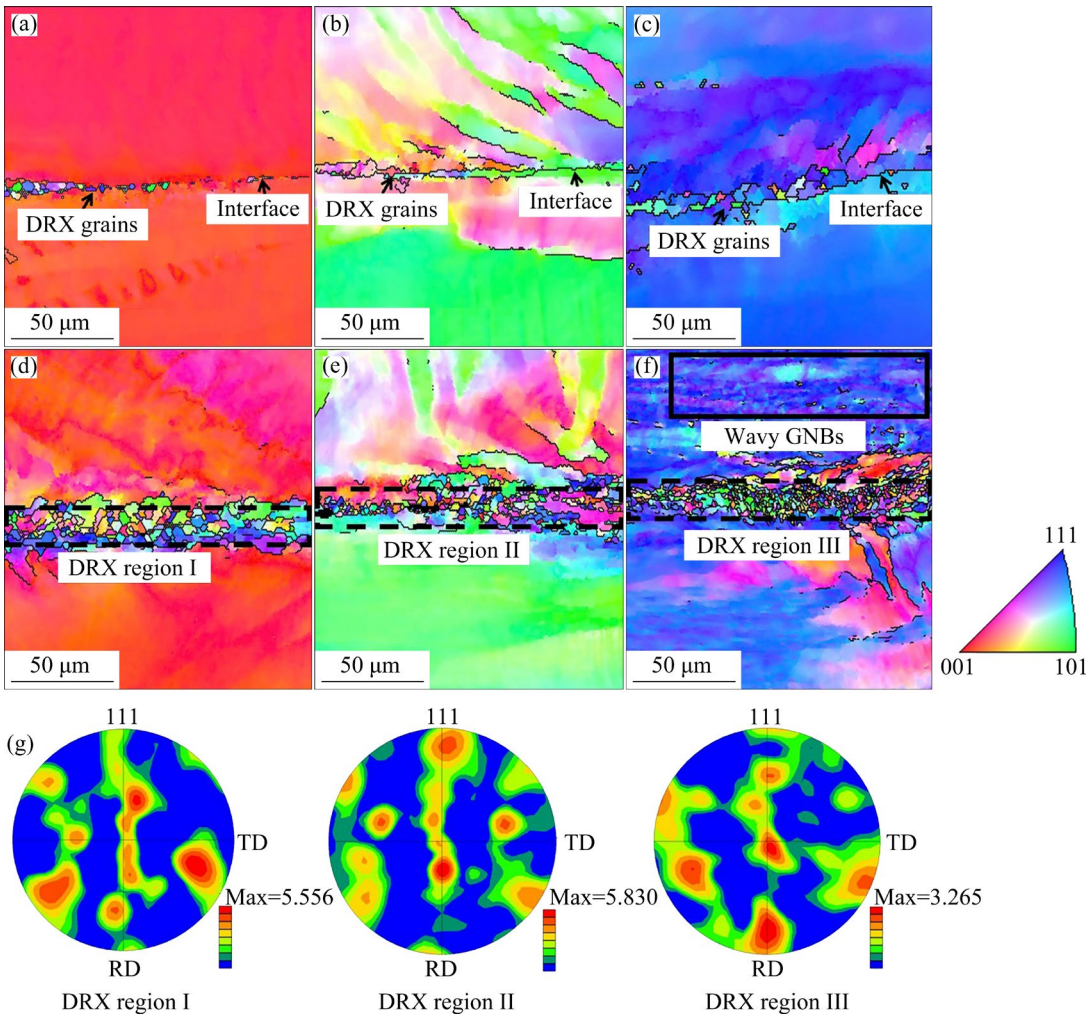

Fig. 3 IPF maps of Cu single crystal joints: (a−c) Joints welded at 200 J with grain orientations of [001], [101], and [111], respectively; (d−f) Joints welded at 700 J with grain orientations of [001], [101], and [111], respectively; (g) PFs of DRX regions marked in (d−f)

interfaces was driven by continuous welding energy inputs. The grain orientation in the DRX regions, analyzed in Fig. 3(g), showed a random distribution in the interfacial regions covered with refined grains. According to HUANG and LOGÉ [27], discontinuous dynamic recrystallization (DDRX) involved the nucleation and growth of strain-free grains, inducing a randomizing effect on crystallographic texture. The PFs indicated that the ultrasonic superimposed high-strain-rate deformation during UW had a negligible impact on the formation of texture at interfaces. The interfacial microstructures for [001], [101], and [111] joints exhibited isotropic grain evolution dominated by DDRX. Typically, high-strain-rate deformation for pure Cu resulted in grain refinement through continuous dynamic recrystallization (CDRX) because of the rapid accumulation and pile-up of intragranular dislocations [24]. In contrast, the DDRX phenomenon observed in this research could be attributed to the ultrasonically excited dislocations that drove grain boundary migration.

3.2 Dislocation and DRX behaviors at interfaces

To further investigate the orientation-dependent microstructures at the interface, samples welded at 200 J were characterized using TKD and TEM for the microstructural analysis of interfacial micro-regions, as depicted in Figs. 4−6. Prior to the complete elimination of interfacial gaps in [001] and [111] joints, the initial Cu single crystal substrates underwent progressive orientation rotation because of frictional deformation, resulting

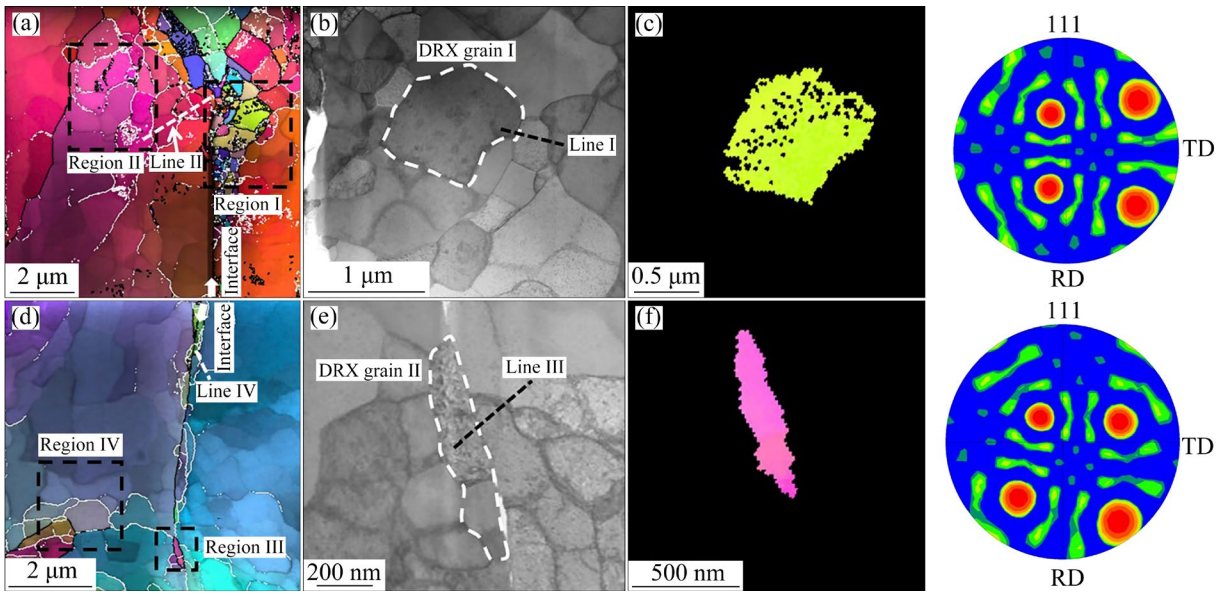

Fig. 4 Interfacial morphologies of Cu single crystal joints welded at 200 J: (a, d) IPF superimposed IQ maps for joints with [001] and [111] grain orientations, respectively; (b, e) STEM images for dislocation substructures and interfacial DRX grains of Regions I and III marked in (a) and (d), respectively; (c, f) Orientation analysis results of DRX grains in joints with grain orientations of [001] and [111], respectively

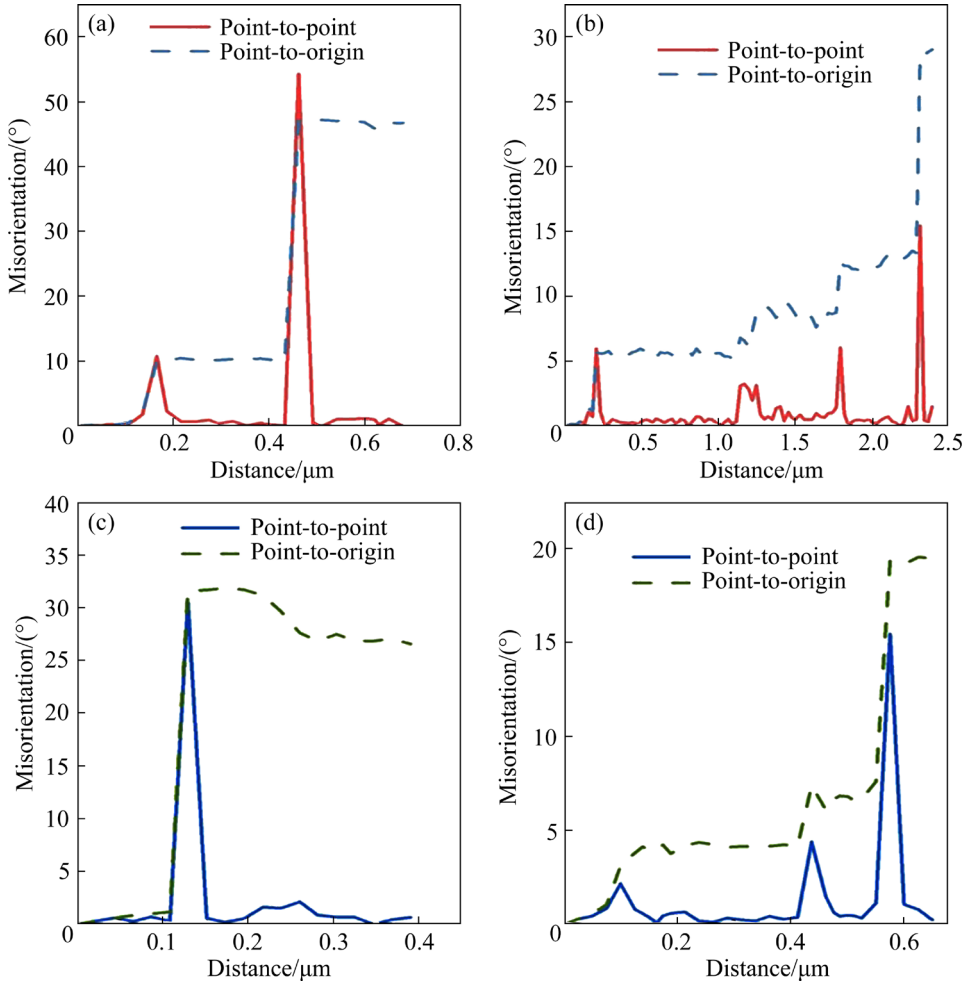

Fig. 5 Misorientation profiles of Line I (a), Line II (b), Line III (c), and Line IV (d) marked in Fig. 4

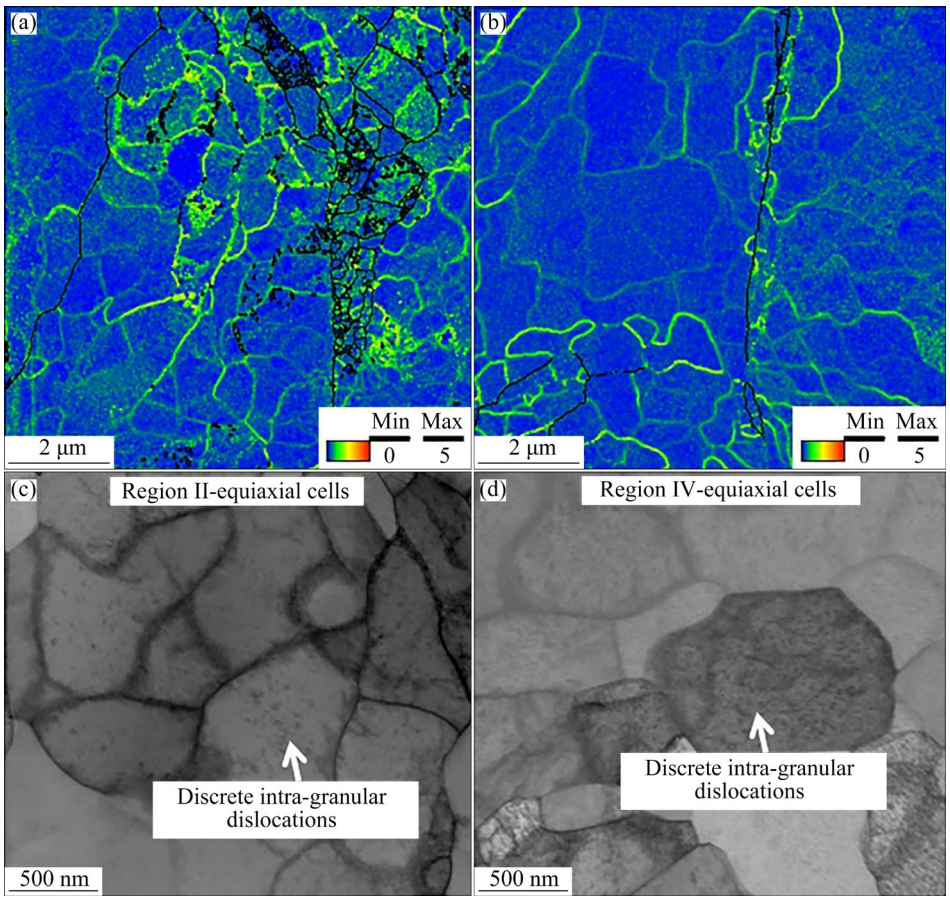

Fig. 6 (a, b) KAM maps for joints with [001] and [111] grain orientations, respectively; (c, d) STEM images of Regions II and IV marked in Fig. 4, respectively

in several ultrafine DRX grains with a sub-micro scale near the interface. Orientation analysis of DRX regions, shown in Figs. 4 and 5, revealed that the nucleation and growth of DRX grains in [001] and [111] joints led to the randomization of the initial texture, with significant misorientation between DRX grains and initial single crystal (Lines I and III).

In addition, several ultra-fine grains developed through progressively accumulative misorientation from the initial single crystal to their boundaries, as evident in the misorientation profiles over Lines II and IV. This evolution was commonly attributed to CDRX mechanisms because of progressive lattice rotation [28].

In UW, the high-frequency vibration of the sonotrode induced frictional deformation with a high $\ln Z$ value (>30) at the interfaces [29]. According to the deformation map established by TIAMIYU et al [30], when pure Cu was subjected to a deformation condition with a relatively high $\ln Z$ value (>25) and large strains (>1.5), newly fine grains were primarily generated in the form of CDRX through the accumulation of intra-granular dislocations. Conversely, DDRX represented dominance in the grain refinement process for [001] and [111] joints under an interfacial deformation condition of ultrasonic superimposed on the high-strain-rate. This implied that the ultrasonic excitation performed a characteristic role in the intra-granular dislocation behaviors, as confirmed by the kernel average misorientation (KAM) maps shown in Figs. 6(a, b). The differences in KAM values between the grain boundaries and the grain interiors indicated that ultrasonic vibration provided sufficient driving force for the movement of dislocations within the grains.

Differential activation of dislocation slip systems constitutes an intrinsic factor for the formation of different dislocation substructures in Cu single crystals with [001] and [111] orientations [31]. However, as shown in Figs. 6(c, d), ultrasonic-accelerated dislocation motion altered the intrinsic dependence between deformation microstructures

and initial grain orientation, leading to similar equiaxial dislocation cells and discrete intra-granular dislocations.

The microstructures and grain orientation in the interfacial micro-regions of [101] joints welded at 200 J were characterized using TKD and TEM, as shown in Fig. 7. The rotation of the initial single crystal and the ultra-fine DRX grain layer were also observed before the complete weld formation. According to the friction research on Cu single crystal by TARASOV et al [32], strain inhomogeneity of [111] and [110] orientations facilitated the formation of shear bands and continuous misorientation between the DRX grains and the matrix. The analysis of grain orientation (Fig. 7) and misorientation profiles (Fig. 8) indicated progressive lattice rotation and substantial misorientation accumulation at grain boundaries for [101] joints. Ultra-fine grains with random re-orientations dominated in the DRX regions, suggesting that DDRX was the primary mechanism for the grain refinement in [101] joints. Combining

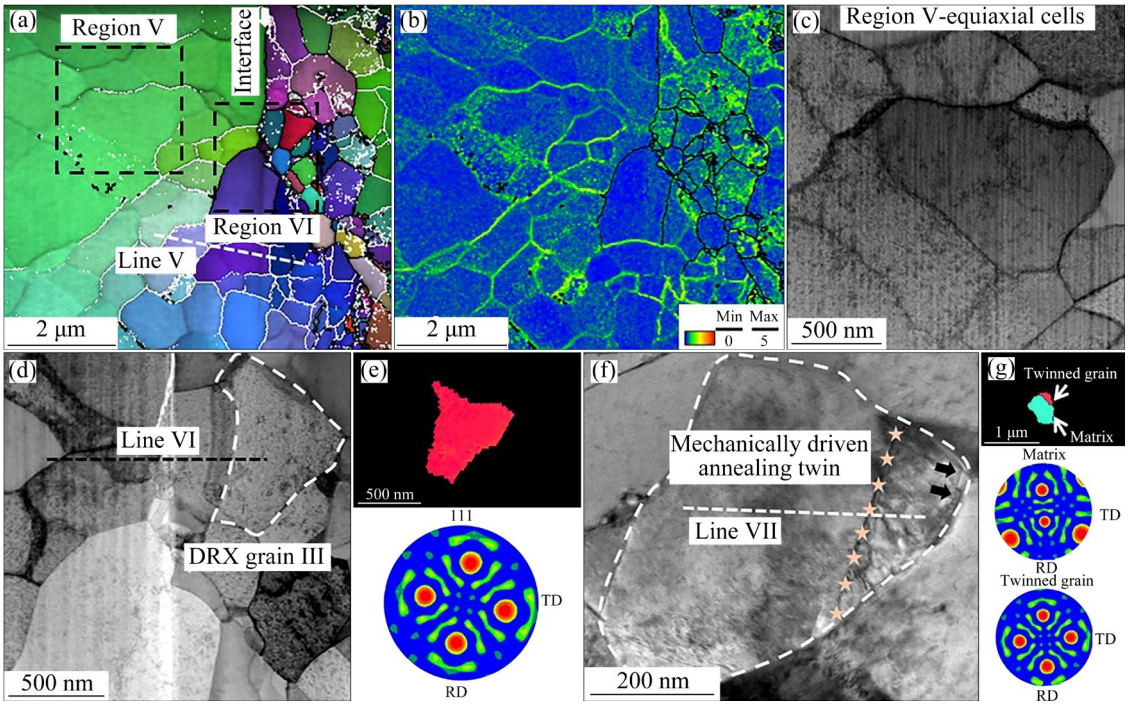

Fig. 7 Interfacial morphologies of joints welded at 200 J with grain orientation of [101]: (a, b) IPF superimposed IQ and KAM maps, respectively; (c, d) STEM images for dislocation substructures and interfacial DRX grains of Regions V and VI marked in (a), respectively; (e) Grain orientation analysis results of DRX grain III; (f, g) TEM characterization and orientation analysis results of twins, respectively

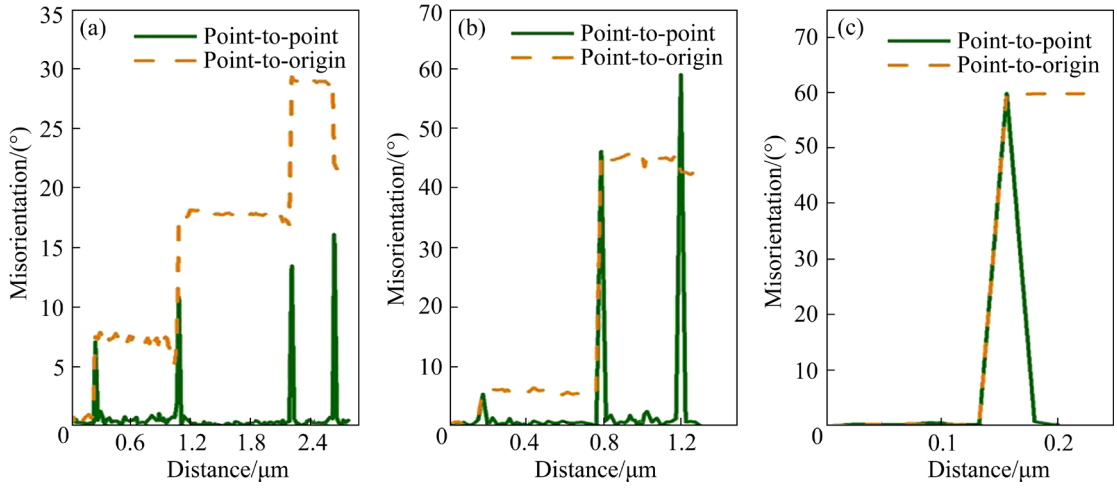

Fig. 8 Misorientation profiles of Line V (a), Line VI (b), and Line VII (c) marked in Fig. 7

the KAM profiles and STEM characterization results of initial single crystal regions, the enhanced intra-granular dislocation motion resulted in higher KAM values in low-angle grain boundaries and the formation of equiaxial cells induced by the activation of highly symmetric slip systems. The dislocation substructures and DRX mode exhibited an isotropic microstructural feature for [001], [101], and [111] joints welded at 200 J.

Furthermore, in contrast to massive nano-sized twins induced by typical high-strain-rate deformation [16], several mechanically annealing twins generated by boundary migration in the DRX regions reached sub-micro size, as shown in Fig. 7(f). The grain orientation and misorientation profiles revealed that the twin boundary in this research was identified as the typical Σ3[111]60° coherent twin boundary. According to AN et al [33] and LIU et al [34], this twinning mode was activated by extensive strain accumulation at the grain boundaries during dislocation motion and DDRX process. In UW, the ultrasonic vibration promoted the motion of intra-granular dislocations toward the grain boundaries, resulting in the formation of mechanically driven annealing twins during grain growth in the DRX regions.

Figures 9 and 10 show interfacial morphologies of [001], [101], and [111] joints welded at 700 J. With continuous welding inputs, the expansion of nascent DRX grains fully filled the unwelded regions because of the continuous stored deformation energy and frictional heat. Based on the research of BROWN et al [12], the size of refined grain structures could reach nanoscale after deformation at a high-strain-rate of 10^3 s^{-1}. In UW, the interfacial DRX grains were significantly larger than those formed during typical high-strain-rate deformation of pure Cu. However, the DRX regions consisted of the re-oriented grains or sub-grain structures near the microscale, and the refined grain structures exhibited no preferential orientation. This was attributed to the enhanced dislocation motion and boundary migration under ultrasonic excitation. The KAM maps in Figs. 9(d−f) show higher KAM values along the grain boundaries, indicating high mobility of intra-granular dislocations even with differential activation of slip systems in joints with various orientations.

The dislocation substructures in nascent DRX grains with [001], [101], and [111] orientations in Cu single crystal joints were characterized by STEM, as shown in Fig. 10. The isotropic micro-structural features of discrete dislocations and boundary migration were also found in the re-oriented grains for joints with various orientations. The appearance of tortuous pre-existing boundaries

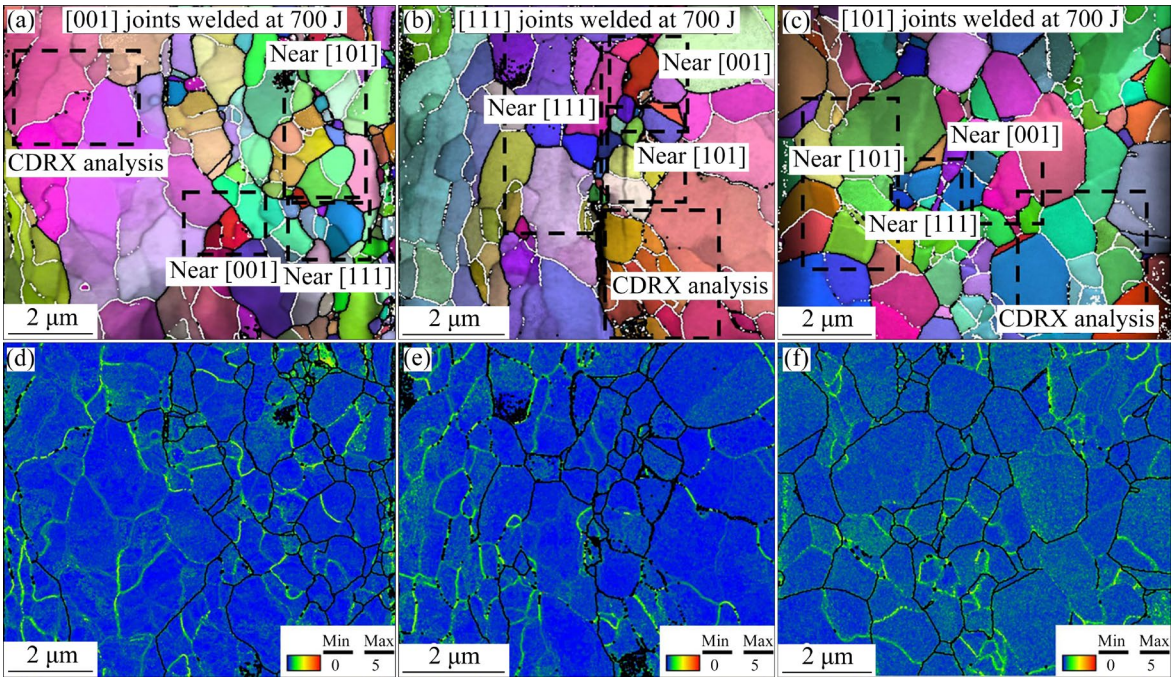

Fig. 9 Interfacial morphologies of Cu single crystal joints welded at 700 J: IPF superimposed IQ (a−c) and KAM (d−f) maps for joints with [001] (a, d), [111] (b, e), and [101] (c, f) grain orientations, respectively

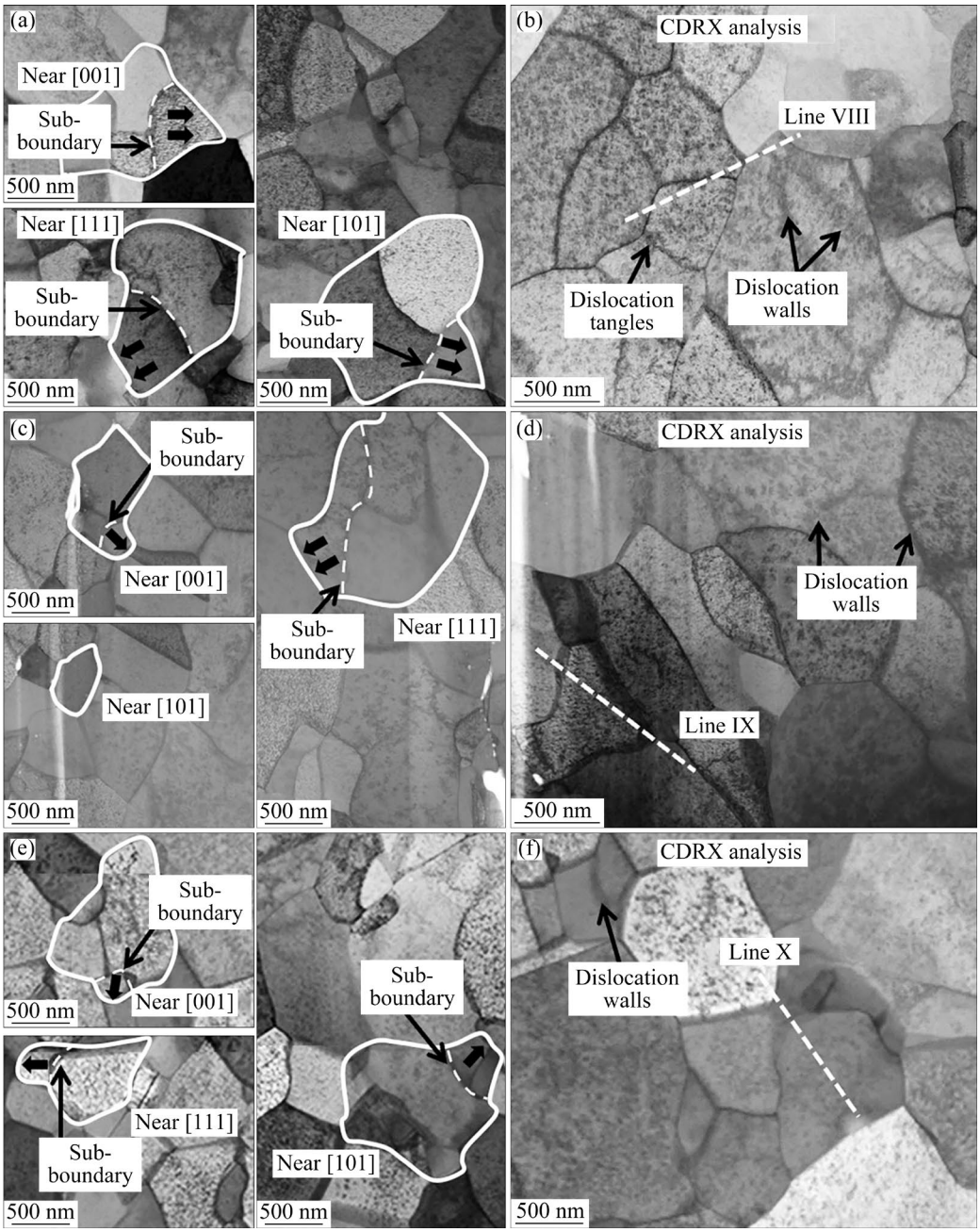

Fig. 10 (a, c, e) STEM images for DRX grains with [001], [111], and [101] orientations, respectively; (b, d, f) TEM images for CDRX regions marked in Figs. 9(a−c), respectively

generated by the boundary migration implied a recrystallization process involving the formation of strain-induced sub-boundaries. Subsequent grain refinement in the nascent re-oriented grains predominantly followed a DDRX mode.

Additionally, CDRX analysis in the specific regions for [001], [101], and [111] joints indicated that the homogeneous initiation of intra-granular dislocations led to the development of dislocation tangles, dislocation walls, and sub-grain boundaries in the nascent re-oriented grains. In Fig. 11, the misorientation profiles further revealed that the evolution of dislocation substructures induced progressive lattice rotation, ultimately refining the grains through a CDRX mode. In comparison with dislocation and DRX behaviors in joints with various orientations, identical dislocation substructures and grain refinement modes indicated an isotropic evolution in the interfacial regions even under the aggravated strain accumulation induced by a higher welding energy input.

3.3 XRD patterns and microhardness

The grain orientation and microhardness were examined to further analyze the evolution characteristics of microstructures and mechanical properties at the interfaces, as shown in Figs. 12 and 13. The diffraction peaks were localized at 2θ values of 50.4°, 74.1°, and 43.2° for welding substrates with [001], [101], and [111] orientations, respectively. The grain orientations for Cu single crystal joints welded at 200 and 700 J are shown in Fig. 12(b). The initial orientation of Cu single crystals retained high intensities of diffraction peaks. Similar to the grain re-orientation and poly-crystallization observed in the interfacial regions using EBSD and TKD characterization, the intensity of the weak diffraction peaks in the Cu single crystal joints with various orientations exhibited an isotropic gradual enhancement with the increase in welding energies.

The Vickers microhardness in the interfacial FIB-prepared micro-regions was analyzed by the nanoindentation test, as shown in Fig. 13. For joints

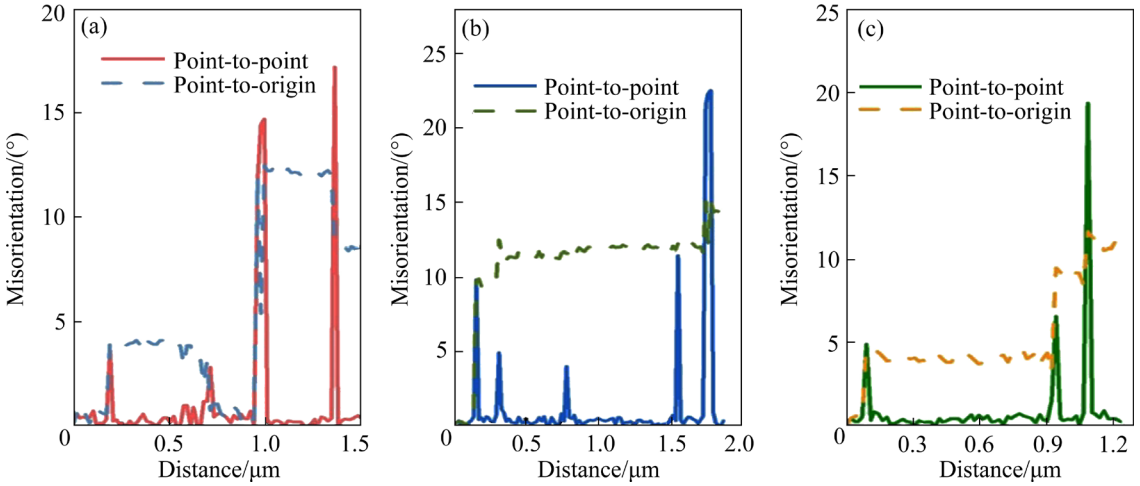

Fig. 11 Misorientation profiles of Line VIII (a), Line IX (b), and Line X (c) marked in Fig. 10

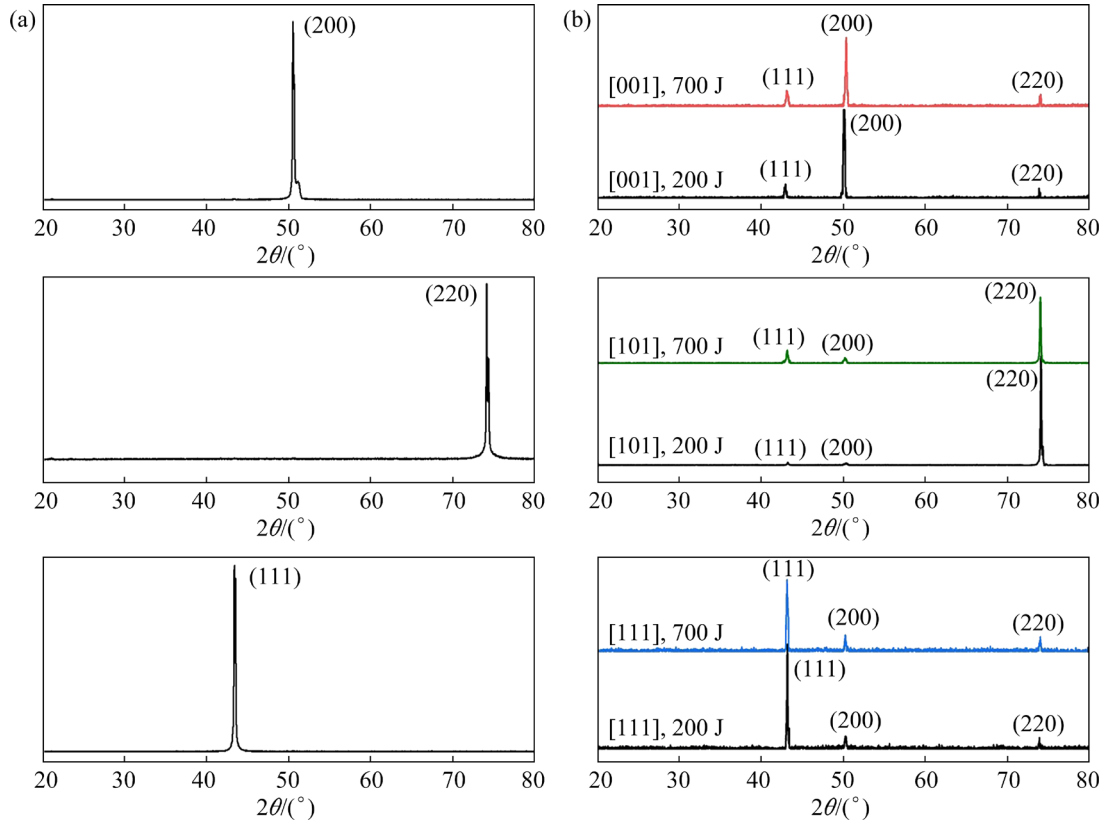

Fig. 12 XRD patterns of Cu single crystal joints before (a) and after (b) UW

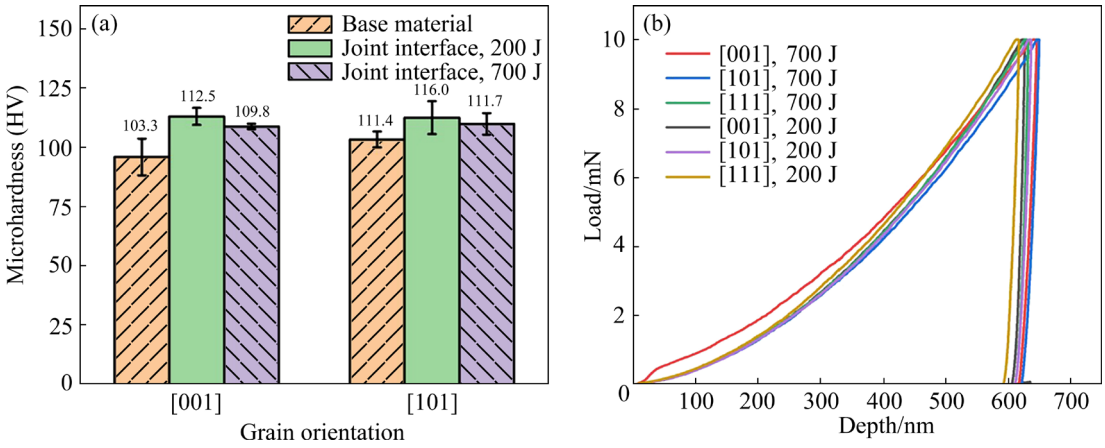

Fig. 13 Vickers microhardness values (a) and nanoindentation curves (b) for Cu single crystal joints welded at 200 and 700 J with different grain orientations

welded at 200 J, the development of ultra-fine dislocation substructures and re-oriented grains improved microhardness at the interfaces. As the welding energy increased to 700 J, ultrasonic-driven dislocation motion and frictional heat facilitated boundary migration. The nascent dislocation substructures and re-oriented grains progressively increased in size, reaching nearly microscale, which led to a slight reduction in microhardness at the joint interfaces. Identical microhardness variation provided additional evidence that the microstructures of single crystal joints underwent an isotropic evolution during the ultrasonic superimposed high-strain-rate deformation.

3.4 Welding quality assessment by X-CT analysis

For conventional solid bonding of Cu to Cu, the surface diffusion coefficient on the [111] orientation is 3−4 orders of magnitude larger than that on other orientations, which indicated that joints welded using the [111] orientation exhibit superior welding quality under the same bonding process [35]. To assess the differences in welding quality among the ultrasonically welded joints with various orientations, X-CT analysis was conducted, and the results are shown in Fig. 14. At a welding energy of 200 J, local unbonded regions occurred in the [001], [101], and [111] joints because of insufficient material flow at the interface. The differential diffusion rates and activation of slip systems caused by orientation constraints did not result in discrepancies in the welding quality of Cu single crystal joints.

As the welding energy increased to 700 J, continuous frictional deformation progressively expanded the bonded regions across the welding interfaces. X-CT analysis results of joints with various orientations revealed an isotropic trend in welding quality. In UW, the interfacial regions underwent a three-stage evolution involving fragmentation of oxide, material flow, and atomic-diffusion [36]. The microstructural analysis of Cu single crystal joints showed that a DRX layer with random orientations formed initially at the stage of material flow. In the subsequent atomic-diffusion stage, the re-oriented grains mutually contacted to develop reliable bonding at the interfaces. Consequently, ultrasonic vibration induced an identical microstructure of dislocation substructures and DRX grains by altering orientation constraints. This reduced the difference in diffusion rates among various orientations, contributing to the isotropic evolution of welding quality for Cu single crystal joints.

4 Discussion

4.1 Isotropic dislocation behaviors induced by ultrasonic excitation

The variation in dislocation motion caused by the orientation constraints was the intrinsic factor for the formation of different dislocation configurations. The tendency for partial dislocations to either separate or incorporate affects the cross-slip behavior under varying activation states of slip systems. As a result, the transformation of dislocation slip modes from a planar slip to a wavy

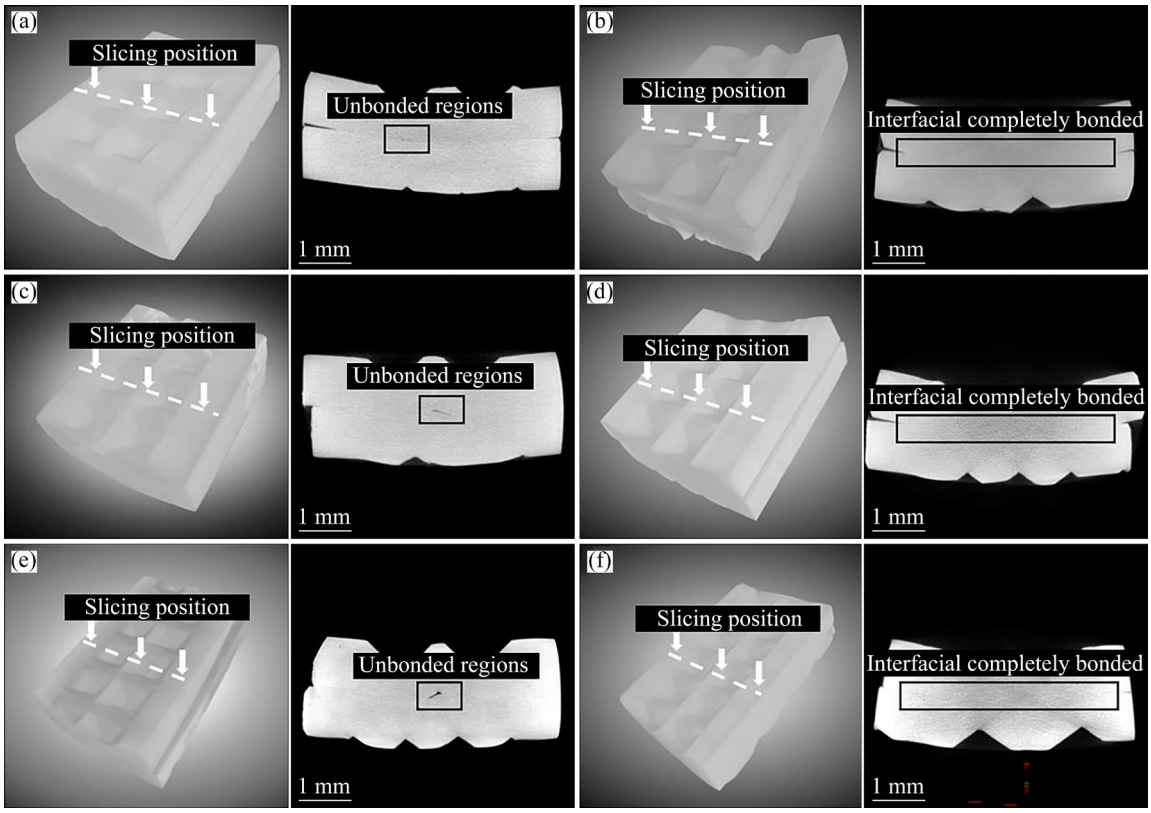

Fig. 14 X-CT scanning patterns of Cu single crystal joints: (a, c, e) Joints welded at 200 J with grain orientations of [001], [101], and [111], respectively; (b, d, f) Joints welded at 700 J with grain orientations of [001], [101], and [111], respectively

slip occurred by enhancing the cross-slip of dislocations [25].

In typical plastic deformation of pure Cu, dislocation configurations evolve from lamellar GNBs to equiaxed dislocation cells with increasing the number of symmetric slip systems. In contrast, an isotropic dislocation substructure characterized by equiaxed dislocation cells was observed simultaneously in the [001], [101] and [111] joints. Dislocation dynamics simulation by SIU et al [17] demonstrated that ultrasonic excitation enabled the dislocations to travel longer distances, and periodic superimposition of oscillation stress and static stress increased the probability of cross-slip. Additionally, the formation of excessive vacancies during UW provided the additional driving force for the dislocation motion, and accelerated the polygonization of dynamic recovery [6]. KANG et al [20] further indicated that ultrasonic vibration caused an inhomogeneous softening among grains with various orientations, and grains with a hard orientation might experience more pronounced ultrasonic effects.

In UW, ultrasonic excitation in the interfacial regions weakened intra-granular dislocation entanglement at the high-strain-rate, and altered constraints on cross-slip imposed by the characteristic orientations. Thus, the isotropic dislocation behavior was observed, driven by the enhanced dislocation motion and cross-slip induced by ultrasonic excitation.

4.2 Preferred DRX mode under ultrasonic superimposed high-strain-rate deformation

UW involves applying ultrasonic vibration and pressure, leading to intense shear plastic deformation as well as considerably elevated temperature at the interfaces. The Z parameter, combining strain rate and temperature during plastic deformation, is typically used to relate process conditions to DRX modes in metals [37]. According to the previous research, the $\ln Z$ value of interfacial friction deformation exceeded 30, and the maximum shear strain within a single welding cycle could reach 1.54 [29]. The strain–Z microstructure map indicated that high-Z processes

predominantly led to deformation twinning and CDRX under low and high strain conditions, respectively [37]. In contrast, the massive bulging boundaries observed in the recrystallized grains suggested that strain-induced boundary migration of DDRX mode dominated in the interfacial regions.

SIU et al [17] indicated that periodic effects of ultrasonic vibration facilitated the cross-slip of dislocation and weakened dislocation pile-up during plastic deformation. In this research, ultrasonic excitation accelerated intra-granular dislocation motion toward grain boundaries, creating a difference in stored energy that provided a prerequisite for DDRX. The nucleation stage of DDRX was analyzed, and the results are shown in Fig. 15. The stored energy difference between adjacent grains drove the initial grain boundary to bow out into Grain II side, generating a sub-grain boundary on Grain I side. The driving force, i.e. the stored energy difference (ΔE) can be calculated using Eq. (1) [38]:

$$\Delta E=0.5\Delta\rho Gb^2 \tag{1}$$

where $\Delta\rho$ represents the dislocation density difference between both sides of the grain boundary; G is the shear modulus, which is 48 GPa for Cu [39]; b represents the magnitude of Burgers vector (0.256 nm for perfect dislocation). By analyzing the dislocation density statistics of Grains I and II, ΔE for the case in Fig. 15 can be calculated to be 3.5×10^5 J/m^2.

The criterion for strain-induced grain migration is given by [38]

$$\Delta E \geq 2\gamma/R \tag{2}$$

where γ is grain boundary energy with a value of 0.4 J/m^2 for the sub-micro sized Cu grains [40]; R represents the curvature radius of the bulging boundary, which was measured to be approximately 2.5 μm for the case in Fig. 15. Substituting specific values into Eq. (2), the critical stored energy difference required to trigger the phenomena of strain-induced grain boundary migration is 3.1×10^5 J/m^2.

Therefore, the ultrasonic vibration-induced acceleration of intra-granular dislocation motion created a sufficient dislocation density difference across the grain boundary. This was the intrinsic reason that led to DDRX being the prominent mode of grain refinement in the interfacial regions.

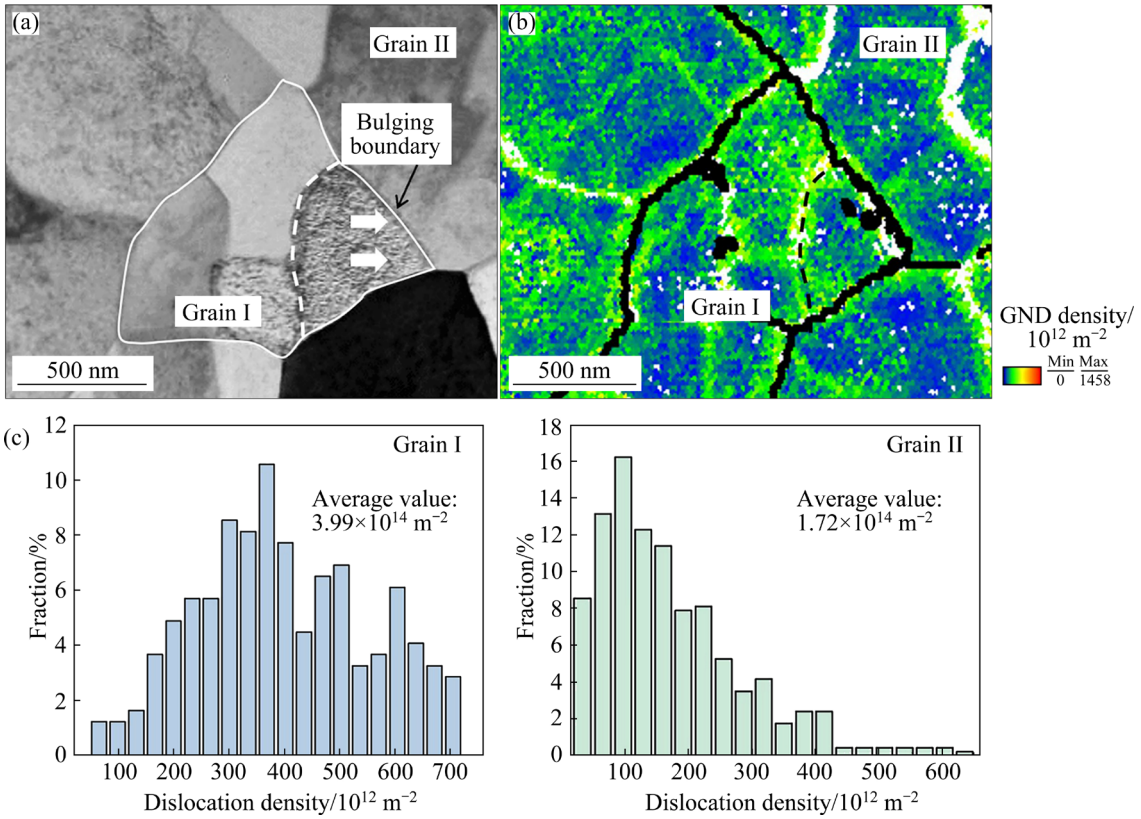

Fig. 15 DDRX mode analysis results in interfacial regions: (a) STEM image for bulging boundary; (b) Dislocation analysis map; (c) Dislocation density profiles for adjacent Grains I and II during DDRX process

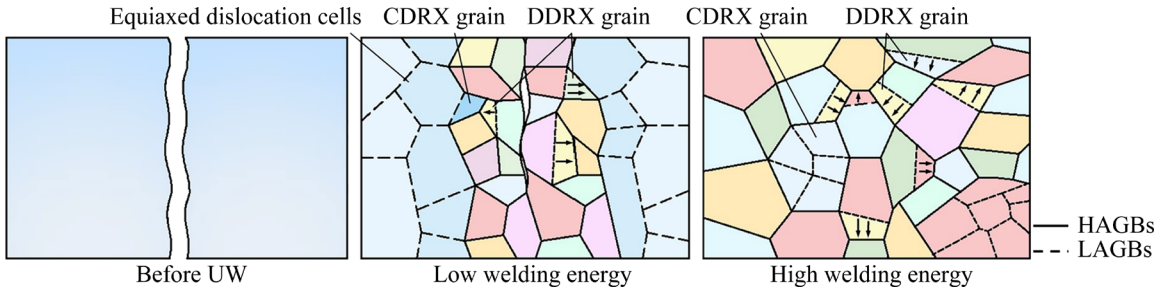

Fig. 16 Schematics for microstructural evolution of Cu single crystal joints under different conditions

Moreover, the identical dynamic recrystallization mode for [001], [101], and [111] joints observed in Figs. 4 and 9 further confirmed that ultrasonic excitation weakened orientation constraints on intra-granular dislocation motion, resulting in the isotropic evolution of joint microstructures and properties.

4.3 Isotropic microstructure evolution of Cu single crystal joints during UW

Based on the analysis of microstructural and welding quality for [001], [101], and [111] joints, the weld formation represents an isotropic feature, as illustrated in Fig. 16. For a low welding energy input, insufficient frictional deformation inhibited the complete extension of the bonding regions, and the interfacial gaps were still observed in the Cu single crystal joints. Ultrasonic excitation altered the correlation between dislocation substructures and orientation, and drove the boundary migration by enhancing intra-granular dislocation motion. Correspondingly, the ultrasonic superimposed high-strain-rate deformation produced orientation-independent microstructures, characterized by equiaxed dislocation cells, DDRX grains, few CDRX grains and mechanically driven annealing twins in the interfacial regions.

As the welding energy increased, continuous ultrasonic vibration enabled the DRX regions to fill the interfacial gaps, and dramatically expanded net welded areas. The homogeneous initiation of dislocations within the grains resulted in the isotropic morphologies of dislocations in the nascent re-oriented grains, and interfacial microstructures were mainly refined by the DDRX modes. This indicated that even under the condition of intense deformation and substantial dislocation accumulation at the interfaces, ultrasonic vibration could still weaken the intra-granular dislocation entanglement and facilitate dislocation-driven grain boundary migration.

5 Conclusions

(1) At a low welding energy, the orientation-independent microstructures of the equiaxed dislocation cells and DDRX grains dominated in the interfacial regions of Cu single crystal joints. As the welding energy increased, the interfacial regions were completely covered by the refined DRX grains.

(2) The randomly oriented recrystallized layer weakened the difference in plastic deformation and diffusion rates among various orientations, contributing to the isotropic evolution of micro-hardness and welding quality for joints with various orientations.

(3) Ultrasonic excitation weakened the intra-granular dislocation entanglement and altered the constraints on cross-slip imposed by the characteristic orientations, which facilitated the homogeneous dislocation nucleation and motion under the loading mode of high-strain-rate, serving as the intrinsic factor for the isotropic evolution feature for Cu single crystal joints.

CRediT authorship contribution statement

Qiu-chen MA: Conceptualization, Investigation, Formal analysis, Funding acquisition, Writing − Original draft; **Jing-yuan MA:** Conceptualization, Investigation, Modelling; **Xiao-xiong ZHENG:** Supervision, Writing − Review & editing; **Xu-kai HUANG:** Investigation, Writing − Review & editing; **Hong-jun JI:** Funding acquisition, Resources, Supervision, Writing − Review & editing.

Declaration of competing interest

The authors declare that they have no known

competing financial interests or personal relationships that could have appeared to influence the work reported in this paper.

Acknowledgments

This work was supported by the National Natural Science Foundation of China (Nos. 52175310, 52232004), the Launch Research Program of Fuzhou University, China (No. XRC-23083), the Education & Research Project of Fujian Province, China (No. JAT231003), and the Open Test Fund for Valuable Instruments and Equipment of Fuzhou University, China (No. 2024T036).

References

[1] CHENG Xian-ming, YANG Ke, LIU Si-zhan, JI Shan-lin, WANG Jian. Microstructure and mechanical properties of ultrasonic welded copper to aluminum cables joints [J]. Transactions of Nonferrous Metals Society of China, 2023, 33: 3027−3038.

[2] MA Qiu-chen, SONG Cheng, ZHOU Jian-li, ZHANG Lin, JI Hong-jun. Dynamic weld evolution during ultrasonic welding of Cu−Al joints [J]. Materials Science and Engineering: A, 2021, 823: 141724.

[3] MA Qiu-chen, MA Jing-yuan, ZHOU Jian-li, JI Hong-jun. Intrinsic dependence of welding quality and recrystallization on the surface-contacted micro-asperity scale during ultrasonic welding of Cu−Cu joints [J]. Journal of Materials Research and Technology, 2022, 17: 353−364.

[4] IWAMOTO C, OHTANI Y, HAMADA K. Microstructure variation in the ultrasonic bonding process between Al sheets observed by in-situ transmission electron microscopy [J]. Scripta Materialia, 2023, 234: 115560.

[5] GUNDUZ I E, ANDO T, SHATTUCK E, WONG P Y, DOUMANIDIS C C. Enhanced diffusion and phase transformations during ultrasonic welding of zinc and aluminum [J]. Scripta Materialia, 2005, 52: 939−943.

[6] HU Yan-ying, LIU Hui-jie, FUJII H, ARAKI H, SUGITA K, LIU Ke. Ultrasonic-induced excess vacancies in friction stir processing and exploration of acoustoplastic effect [J]. Scripta Materialia, 2020, 185: 117−121.

[7] ZHANG Zi-jiao, WANG Kai-feng, LI Jing-jing, YU Qian, CAI W. Investigation of interfacial layer for ultrasonic spot welded aluminum to copper joints [J]. Scientific Reports, 2017, 7: 12505.

[8] LIN J Y, NAMBU S, KOSEKI T. Interfacial phenomena during ultrasonic welding of ultra-low-carbon steel and pure Ti [J]. Scripta Materialia, 2020, 178: 218−222.

[9] LI Zhen, LI Xin, HUANG Zhi-yuan, ZHANG Zhen-xuan, LIANG Xiong, LIU Huan, LIAW P K, MA Jiang, SHEN Jun. Ultrasonic-vibration-enhanced plasticity of an entropic alloy at room temperature [J]. Acta Materialia, 2022, 225: 117569.

[10] DAI Xiang, SHI Lei, TIAN Chun-yan, WU Chuan-song, GAO Song. Effect of ultrasonic vibration on microstructures and mechanical properties of friction stir welded 2195 Al−Li alloy [J]. Transactions of Nonferrous Metals Society of China, 2024, 34: 80−93.

[11] NIU Ran-ming, AN Xiang-hai, LI Lin-lin, ZHANG Zhe-feng, MAI Yiu-wing, LIAO Xiao-zhou. Mechanical properties and deformation behaviours of submicron-sized Cu−Al single crystals [J]. Acta Materialia, 2022, 223: 117460.

[12] BROWN T L, SALDANA C, MURTHY T G, MANN J B, GUO Y, ALLARD L F, KING A H, COMPTON W D, TRUMBLE K P, CHANDRASEKAR S. A study of the interactive effects of strain, strain rate and temperature in severe plastic deformation of copper [J]. Acta Materialia, 2009, 57: 5491−5500.

[13] WINTHER G, HUANG X. Dislocation structures. Part II: Slip system dependence [J]. Philosophical Magazine, 2007, 87: 5215−5235.

[14] HANSEN N, HUANG X, PANTLEON W, WINTHER G. Grain orientation and dislocation patterns [J]. Philosophical Magazine, 2006, 86: 3981−3994.

[15] CAI S S, LI X W, TAO N R. Orientation dependence of deformation twinning in Cu single crystals [J]. Journal of Materials Science & Technology, 2018, 34: 1364−1370.

[16] VOISIN T, GRAPES M D, LI T T, SANTALA M K, ZHANG Y, LIGDA J P, LORENZO N J, SCHUSTER B E, CAMPBELL G H, WEIHS T P. In situ TEM observations of high-strain-rate deformation and fracture in pure copper [J]. Materials Today, 2020, 33: 10−16.

[17] SIU K W, NGAN A H W, JONES I P. New insight on acoustoplasticity—Ultrasonic irradiation enhances subgrain formation during deformation [J]. International Journal of Plasticity, 2011, 27: 788−800.

[18] BACHURIN D V, MURZAEV R T, NAZAROV A A. Discrete dislocation simulation of the ultrasonic relaxation of non-equilibrium grain boundaries in a deformed polycrystal [J]. Ultrasonics, 2021, 117: 106555.

[19] KANG Jia-rui, LIU Xun, XU Ming-jie. Plastic deformation of pure copper in ultrasonic assisted micro-tensile test [J]. Materials Science and Engineering: A, 2020, 785: 139364.

[20] KANG Jia-rui, LIU Xun, NIEZGODA S R. Crystal plasticity modeling of ultrasonic softening effect considering anisotropy in the softening of slip systems [J]. International Journal of Plasticity, 2022, 156: 103343.

[21] NI Z L, YANG J J, WANG X X, HUANG L, YE F X. Formation of refined grain size less than 5 nm and nano-sized undulations in the bonding interface region of an ultrasonic spot welded Cu/Ni joint [J]. Metallurgical and Materials Transactions A, 2020, 51: 5606−5611.

[22] LIN J Y, HU K C, HSIEH T L, CHU H E. Improved interfacial strength of Ti/Ti ultrasonic welds by introducing $\alpha/\beta/\alpha$ heterogeneous bonding interface [J]. Scripta Materialia, 2023, 237: 115724.

[23] HANSEN N, HUANG X. Microstructure and flow stress of polycrystals and single crystals [J]. Acta Materialia, 1998, 46: 1827−1836.

[24] SAKAI T, BELYAKOV A, KAIBYSHEV R, MIURA H, JONAS J J. Dynamic and post-dynamic recrystallization under hot, cold and severe plastic deformation conditions [J]. Progress in Materials Science, 2014, 60: 130−207.

[25] AN X H, WU S D, WANG Z G, ZHANG Z F. Significance of stacking fault energy in bulk nanostructured materials:

Insights from Cu and its binary alloys as model systems [J]. Progress in Materials Science, 2019, 101: 1−45.
[26] ZHAO Yu-hui, ZHAI Ji-qiang, GUAN Yan-jin, CHEN Feng-jiao, LIU Ya, LI Yi, LIN Jun. Molecular dynamics study of acoustic softening effect in ultrasonic vibration assisted tension of monocrystalline/polycrystalline coppers [J]. Journal of Materials Processing Technology, 2022, 307: 117666.
[27] HUANG K, LOGÉ R E. A review of dynamic recrystallization phenomena in metallic materials [J]. Materials & Design, 2016, 111: 548−574.
[28] LEONARD M, MOUSSA C, ROATTA A, SERET A, SIGNORELLI J W. Continuous dynamic recrystallization in a Zn−Cu−Ti sheet subjected to bilinear tensile strain [J]. Materials Science and Engineering: A, 2020, 789: 139689.
[29] MA Qiu-chen, MA Jing-yuan, ZHOU Jian-li, ZHENG Xiao-xiong, JI Hong-jun. Dislocation behavior in Cu single crystal joints under the ultrasonically excited high-strain-rate deformation [J]. Journal of Materials Science & Technology, 2023, 141: 66−77.
[30] TIAMIYU A A, PANG E L, CHEN X, LEBEAU J M, NELSON K A, SCHUH C A. Nanotwinning-assisted dynamic recrystallization at high strains and strain rates [J]. Nature Materials, 2022, 21: 786−794.
[31] SUN Qing-qing, NI Yong, WANG Shu-ai. Orientation dependence of dislocation structure in surface grain of pure copper deformed in tension [J]. Acta Materialia, 2021, 203: 116474.
[32] TARASOV S Y, CHUMAEVSKII A V, LYCHAGIN D V, NIKONOV A Y, DMITRIEV A I. Subsurface structural evolution and wear lip formation on copper single crystals under unlubricated sliding conditions [J]. Wear, 2018, 410/411: 210−221.
[33] AN X H, LIN Q Y, WU S D, ZHANG Z F. Mechanically driven annealing twinning induced by cyclic deformation in nanocrystalline Cu [J]. Scripta Materialia, 2013, 68: 988−991.
[34] LIU Mao, WANG Peng-fei, LU Guo-xing, HUANG Cheng-yao, YOU Zhong, WANG Chien-he, YEN Hung-wei. Deformation-activated recrystallization twin: New twinning path in pure aluminum enabled by cryogenic and rapid compression [J]. iScience, 2022, 25: 104248.
[35] LIU C M, LIN H W, HUANG Y S, CHU Y C, CHEN C, LYU D R, CHEN K N, TU K N. Low-temperature direct copper-to-copper bonding enabled by creep on (111) surfaces of nanotwinned Cu [J]. Scientific Reports, 2015, 5: 9734.
[36] LI H, CHOI H, MA C, ZHAO J Z, JIANG H R, CAI W, ABELL J A, LI X C. Transient temperature and heat flux measurement in ultrasonic joining of battery tabs using thin-film microsensors [J]. Journal of Manufacturing Science and Engineering, 2013, 135: 051015.
[37] LIU Zhi-ying, WANG Hong-ze, HACHÉ M J R, CHU Xin, IRISSOU E, ZOU Yu. Prediction of heterogeneous microstructural evolution in cold sprayed copper coatings using local Zener−Hollomon parameter and strain [J]. Acta Materialia, 2020, 193: 191−201.
[38] ZHANG Jian-yang, XU Bin, HAQ T N, SUN Ming-yue, LI Dian-zhong, LI Yi-yi. Microstructure evolutions and interfacial bonding behavior of Ni-based superalloys during solid state plastic deformation bonding [J]. Journal of Materials Science & Technology, 2020, 46: 1−11.
[39] EDALATI K, HORITA Z. High-pressure torsion of pure metals: Influence of atomic bond parameters and stacking fault energy on grain size and correlation with hardness [J]. Acta Materialia, 2011, 59: 6831−6836.
[40] SUN Y A, LUO Z P, LI X Y, LU K. Effects of stacking fault energy on deformation induced grain boundary relaxation in nanograined Cu alloys [J]. Acta Materialia, 2022, 239: 118256.

单晶铜在超声焊接过程中的各向同性演变特质

马秋晨[1,2,3]，马靖远[2,3]，郑晓雄[2,3]，黄须楷[1]，计红军[2,3]

1. 福州大学 先进制造学院，晋江 362251；
2. 哈尔滨工业大学(深圳) 材料结构精密焊接与连接全国重点实验室，深圳 518055；
3. 哈尔滨工业大学(深圳) 集成电路学院，深圳 518055

摘 要：基于变形显微组织和晶粒取向的关系，分析了 3 种特征取向单晶铜在超声焊接过程中超声叠加高应变速率对位错运动的互斥作用。结果表明，接头组织主要由等轴位错胞和不连续动态再结晶晶粒构成。3 种单晶铜接头在晶粒取向、焊接质量和微观力学性能方面均呈现各向同性的演变趋势。借助储能差异模型进一步分析了主导的位错行为和动态再结晶模式，发现超声激励诱发的晶内高活性位错和均质化位错运动是形成各向同性显微组织和焊接质量的内在因素。

关键词：单晶铜；超声焊接；动态再结晶；位错亚结构；高应变速率变形

(Edited by Wei-ping CHEN)